Design and experimental verification of a bunch length monitor based on coherent Cherenkov diffraction radiation

C. Davut◉, G. Xia◉, O. Apsimon◉, and J. McGunigal◉

The Department of Physics and Astronomy, University of Manchester, M13 9PL Manchester, United Kingdom
and The Cockcroft Institute of Accelerator Science and Technology, WA4 4AD Warrington, United Kingdom

P. Karataev◉

John Adams Institute at Royal Holloway, University of London, Egham, Surrey TW20 0EX, United Kingdom

T. Lefevre◉, S. Mazzoni◉, and E. Senes◉

CERN, CH-1211 Geneva 23, Switzerland

This paper presents the design and experimental commissioning of a noninvasive electron bunch length monitor based on the detection of coherent Cherenkov diffraction radiation (ChDR). The measurement technique effectively eliminates the influence of bunch-by-bunch charge fluctuations, as each detector measures the signal from the same bunch while mitigating the impact of bunch position jitter on the measurements, providing a potential real-time diagnostic tool with significant operational advantages. The sensitivity of the measurements to both bunch length and longitudinal bunch profile was experimentally demonstrated, with results validated against invasive radio frequency deflector measurements at the CLEAR electron test facility at CERN. The ChDR bunch length monitor can be applied to accelerators operating with ultrashort bunches.

I. INTRODUCTION

The Advanced Proton Driven Plasma Wakefield Acceleration Experiment (AWAKE) at CERN [1–4] is an accelerator R&D project in which a 400-GeV proton bunch from the Super Proton Synchrotron is used for the first time to drive beam-based plasma wakefield acceleration [5,6]. The motivation of the AWAKE program is to achieve high accelerating fields to accelerate the externally injected electron bunch while preserving the bunch quality and ultimately produce high brightness and high-energy particle beams for particle physics applications [7–9]. AWAKE Run 2 consists of four phases to reach the ultimate goal that is to provide high-energy electron bunches for particle physics applications such as dark photon searches in fixed target experiments or very high energy *e-p* collider [10–12]. AWAKE Run 2c aims to inject a short electron bunch in between two proton micro bunches to achieve an accelerating field above 0.5 GV/m. Therefore, a noninvasive, real-time bunch length. measurement technique must be provided before injecting the electron bunch into the plasma cell to ensure and maintain bunch quality during the operation [12].

The well-known short bunch length measurement techniques based on radio-frequency deflecting cavities are

excluded as they are destructive [13]. Electro-optical (EO) diagnostics [14] are noninvasive but rely on direct time-domain electric field measurements, which require an additional laser line integrated into the AWAKE beamline. Additionally, the physical limits of the EO crystals for short bunch lengths and a bulky optical measurement setup present challenges.

Measuring the coherent radiation spectrum, where the radiation wavelength is comparable to or longer than the longitudinal bunch size, is a promising and versatile technique that can be applied to a wide range of bunch lengths. This approach enables measurements without a predefined theoretical resolution limit, with experimentally measured bunch lengths ranging from several tens of picoseconds [15] to sub-100 fs [16,17] in the literature. The accuracy of the bunch length measurement depends on the ability to theoretically predict the radiation spectrum generated by a single electron, the characteristics of the detection system (such as detector bandwidth), and the experimental isolation of coherent radiation from any background noise.

The most common and well-studied diagnostic tools that utilize coherent radiation emission are based on transition and diffraction radiation. Transition radiation (TR) is generated when a relativistic charged particle passes through the interface between two media with different dielectric constants, causing a discontinuity in the medium [18]. At this interface, the reflection and refraction of light, described by Fresnel equations, lead to TR emission in both forward and backward directions [19]. Although single-shot spectrometer studies of this phenomenon are documented in the literature [20–22], TR is a destructive technique. Diffraction radiation

(DR) occurs when a charged particle passes near a target material, inducing dynamic polarization in the medium, which results in radiation emission. The calculation of DR follows Huygens's principle of plane-wave diffraction for relativistic charged particles. Similarly to TR, radiation is emitted in two directions when the charged particle passes near the radiator. Common studies involve setups with a slit between screens or a circular hole in a screen [23–25]. However, a significant drawback of DR-based diagnostics is controlling the widespread radiation. More importantly, since both techniques involve a flat metal plate radiator that also acts like a mirror for background radiation—such as synchrotron radiation or short-wavelength wakefields, which depend not only on the bunch length but also on the accelerator's tuning regime—separating coherent DR or TR from all other background radiation is a serious challenge. This often results in systematic deviations in measured results depending on the operation regime. Smith-Purcell radiation (SPr) is produced when a charged particle beam passes above a metallic periodic structure, such as a metallic grating [26–30]. The wavelength of the emitted radiation depends on the specifications of the grating. Consequently, using gratings of different lengths in sequence allows radiation to be emitted at varying wavelengths, covering a wide frequency range and enabling single-shot bunch profile measurements based on SPr [31]. On the one hand, a higher number of sampling frequencies improves the accuracy of bunch profile reconstruction. On the other hand, performing single-shot measurements with such a system introduces complexity, not only in integrating the gratings into the vacuum chamber but also each grating emits radiation at different frequencies, requiring dedicated detectors for each. Moreover, the SPr technique demands additional parameters—such as bunch charge, transverse size, and precise bunch position—to accurately reconstruct the bunch profile. All the techniques mentioned above rely on spectral analysis to reconstruct the bunch profile using complex analytical or iterative phase retrieval algorithms, such as Kramers-Kronig [32] or Gerchberg-Saxton [33]. These algorithms often require initial assumptions about the bunch profile due to the need for extrapolation beyond the measured frequency range to cover the full spectrum.

A diagnostic tool based on coherent Cherenkov diffraction radiation (ChDR) emission is particularly promising. ChDR is generated when a relativistic charged particle moves near and parallel to a dielectric interface, allowing for a noninvasive measurement. Unlike DR, ChDR is emitted at a large angle, providing a monitor that is weakly sensitive to background radiation generated upstream, which copropagates with the bunch. Additionally, ChDR offers a higher photon flux compared to TR and DR because the emission is directly proportional to the length of the radiator [34]. A continuous, coherent ChDR spectrum can be produced by a single radiator, eliminating the need for multiple radiators with varying dimensions, as required for single-shot coherent SPr measurements. Moreover, ChDR theory is more advanced since the polarization current approach (PCA) considers TR, DR, and ChDR collectively, along with their interplay, making the emission theoretically more predictable, whereas the SPr theory focuses solely on its generation mechanism.

The development of a bunch length monitor based on ChDR is relatively new compared to other techniques and has not yet been implemented as an operational diagnostic tool in any accelerator. Nonetheless, coherent ChDR detection has become a strong candidate for noninvasive bunch length diagnostics, with successful experimental validations in recent years [35–42].

In this paper, we describe a compact, noninvasive bunch length monitor based on coherent ChDR, providing a practical solution for real-time longitudinal bunch length measurements. Unlike most coherent-radiation-based diagnostic tools—which typically isolate the bunch length while excluding other key parameters affecting measurement fidelity—our technique employs a dedicated geometry optimized to measure bunch length while simultaneously minimizing the influence of bunch-by-bunch charge fluctuations, bunch position, and angular jitter on the measurements, thereby presents a significant advancement as an operational longitudinal diagnostic tool that does not disrupt beam dynamics. Our measurement method does not rely on complex phase retrieval algorithms to determine the bunch length, thus offering a simpler approach than many other existing ones. The use of Schottky diode detectors to capture the coherent ChDR response allows fast, straightforward, and sensitive detection of short bunch lengths without requiring extensive hardware or large-scale infrastructure modifications. The design, implementation, and experimental validation of the ChDR bunch length monitor for AWAKE Run 2c are discussed, supported by three-dimensional (3D) electromagnetic simulations and a numerical analysis of the theoretical model. Planned upgrades and potential challenges are also considered.

II. COHERENT CHERENKOV DIFFRACTION RADIATION

The interaction of the Coulomb field of a relativistic charged particle with a medium used as a radiator depends on the dielectric properties of the medium and the distance between them. The Coulomb field of the charged particle displaces the electrons on the surface of the radiator, generating dipoles. The generation of these dipoles results in an unstable state and leads to the oscillation of the electrons around the nucleus [43]. Thus, the induced time-varying current is accompanied by electromagnetic radiation emission called polarization radiation.

ChDR refers to the emission of polarization radiation by a charged particle passing in the near vicinity but not in the medium. The radiation is emitted at the characteristic Cherenkov angle within the medium given by

$$\cos(\theta_{\text{ChR}}) = \frac{1}{\beta n(\omega)}, \quad (1)$$

where $\beta = \upsilon/c$ is the speed of the particle in units of the speed of light in vacuum c, ω is the angular frequency, and $n(\omega)$ is the refractive index of the medium. The ChDR spectrum converges to the "classical" Cherenkov radiation (ChR) spectrum when the particle moves through the medium. However, the spectral-angular distribution of ChDR strongly depends on the shortest distance from the medium to the particle trajectory, which is called the impact parameter and differs from that of ChR.

The generation mechanism of ChDR can be defined by different models based on various assumptions about the radiator geometry derived for bunch diagnostics purposes. As a notable model, PCA unifies and calculates the generation of ChDR together with other types of polarization radiation, such as transition and diffraction radiation, using the finite longitudinal size of the radiator, as described in Ref. [44]. The model is based on calculating the spectral-angular distribution of the polarization radiation generated by a relativistic charged particle in rectilinear motion with a Lorentz factor γ passing at a distance b from a prismatic dielectric radiator having a finite length but extends infinitely in the transverse direction. When the radius of the Coulomb field, which is given by

$$r_e = \gamma\beta\lambda/2\pi, \tag{2}$$

satisfies the condition $r_e \geqslant b$, then the dielectric medium is polarized, and polarization radiation is emitted [19].

In reality, the properties of the emitted radiation are more complex when considering that many particles radiate together as a bunch. The radiation generated by a bunch of charged particles is the superposition of radiation generated by each particle within the bunch, which might have constructive or destructive contributions depending on the considered radiation wavelength and the distance between particles [45]. The radiation intensity can be written as

$$I(\omega) = I_e(\omega)[N + N(N-1)F(\omega)], \tag{3}$$

where $\omega = 2\pi f$ is the angular frequency, $I(\omega)$ is the total radiation intensity, $I_e(\omega)$ is the radiation intensity by a single particle, N is the number of particles within the bunch, and $F(\omega)$ is the bunch form factor which represents the statistical characteristics of the longitudinal distribution of the bunch [46]. One should note that the contribution of the transverse component of the bunch form factor becomes negligible in Eq. (3) once the following condition is satisfied:

$$\lambda \gg 2\pi\sigma_r\sin\theta, \tag{4}$$

where λ is the radiation wavelength, σ_r is the transverse bunch size, and θ is the radiation emission angle [47]. For the relativistic case, where $\sin\theta$ approximates to $\theta \approx 1/\gamma$, the transverse component behaves as a constant close to unity. As the experimental parameters used in this paper fulfill this condition, the transverse form factor is neglected in the estimation of coherent radiation.

Considering a bunch having a Gaussian longitudinal distribution, the modulus squared of a Fourier transform applied to the longitudinal charge distribution corresponds to the amplitude of the bunch form factor and is given by

$$F(\omega) = \left| \int_{-\infty}^{\infty} \rho(z)\exp\left(-i\frac{\omega}{c}z\right)dz \right|^2 = \exp\left(-\omega^2\sigma_z^2\right), \tag{5}$$

where σ_z is the standard deviation of the longitudinal charge distribution, which defines the bunch length in seconds, and $\rho(z)$ is the longitudinal charge distribution in a bunch. The first term in Eq. (3) is proportional to N and independent of the bunch form factor. This term is called incoherent radiation

and is uncorrelated radiation of each particle within the bunch. On the other hand, the second term on the right-hand side of the equation depends on the bunch form factor and is proportional to the square of the number of particles. This term is called coherent radiation and is significant when the distance between particles is comparable to or smaller than the radiation wavelength, causing emitted radiation from each particle to match in phase, thus behaving as a single entity.

III. ChDR BUNCH LENGTH MONITOR

In this section, we introduce the underlying methodology of the ChDR bunch length monitor, discuss the principles for optimizing radiators, and determine the Schottky detectors to provide a highly sensitive bunch length diagnostic tool based on the analysis of 3D electromagnetic simulations and theoretical calculations.

A. Bunch length measurement concept

The ChDR bunch length monitor was prototyped based on the electron bunch parameters used in designing the AWAKE Run 2c electron transfer line and the requirements for injecting the electron bunch into the plasma cell. According to the design, the bunch energy is 150 MeV, which is sufficiently high to avoid space-charge effects but low enough to require only a single klystron for acceleration. Furthermore, the optimal bunch profile is considered Gaussian in six dimensions, and the bunch length is determined to be 200 fs to satisfy optimal beam loading and maintain a small energy spread during acceleration [48]. The ChDR bunch length monitor is planned to be positioned at the end of the newly designed electron transfer line, where the 200 fs electron bunch is located before injection into the second plasma cell and prior to any interaction with protons in the AWAKE beamline. With this in mind, the bunch length measurement technique employs two dielectric radiators placed on one side of the bunch along its trajectory. The spectral responses of the coherent ChDR are measured by two Schottky detectors, each operating in a different frequency range. The measured coherent radiation intensity from a Gaussian bunch for each Schottky detector can be written as follows:

$$I_1(\omega_1) = N^2 I_{e1}(\omega_1)\exp\left(-\omega_1^2\sigma_z^2\right),$$
$$I_2(\omega_2) = N^2 I_{e2}(\omega_2)\exp\left(-\omega_2^2\sigma_z^2\right), \tag{6}$$

where, ω_1 and ω_2 are two different frequencies for two detectors, $I_{e1}(\omega_1)$ and $I_{e2}(\omega_2)$ are the ChDR intensities generated by a single electron, $I_1(\omega_1)$ and $I_2(\omega_2)$ are the coherent radiation intensities by the electron bunch. The simultaneous measurements allow us to eliminate the impact of the bunch charge on the measurements by dividing the measured coherent radiation of each detector:

$$\frac{I_1(\omega_1)}{I_2(\omega_2)} = \frac{I_{e1}(\omega_1)\exp\left(-\omega_1^2\sigma_z^2\right)}{I_{e2}(\omega_2)\exp\left(-\omega_2^2\sigma_z^2\right)}. \tag{7}$$

Hence, calculating the single electron response for each detector in its corresponding frequency ranges theoretically enables

us to evaluate the bunch length as follows:

$$\sigma_z = \sqrt{\frac{1}{|\omega_2^2 - \omega_1^2|} \left| \ln \left(\frac{I_1(\omega_1)I_{e2}(\omega_2)}{I_2(\omega_2)I_{e1}(\omega_1)} \right) \right|}, \qquad (8)$$

in a similar manner as given in Ref. [49]. Using the ratio of measured coherent radiation emitted from radiators on the same side of the bunch trajectory to calculate the bunch length minimizes the potential impact of bunch position and angular jitters during the measurements.

B. Optimization of ChDR radiators

The optimization of the radiators was performed by considering the radiator geometry, material, coating, and optimum impact parameters. The geometry of the radiator should enable the emitted ChDR to exit without distortion due to refraction at the output interface of the radiator. Therefore, the emission face of the radiator should be cut at a specific angle, considering the corresponding ChDR emission angle, to prevent such distortion. Since the ChDR emission angle is determined by the dielectric constant, which also affects the emitted radiation intensity, an alumina ceramic with 97.6% Al_2O_3 was chosen as the radiator material [50]. Considering the dielectric permittivity of the chosen alumina, the emitted radiation propagates in and exits the radiator approximately 71° relative to the particle trajectory. Therefore, the radiator angle was determined to be 19°.

One of the critical advantages of alumina is its high and consistent dielectric permittivity across the THz frequency range [51]. Additionally, alumina exhibits a low dissipation factor, tanδ, which is only weakly dependent on temperature, resulting in minimal power absorption up to 1 THz [52]. Alumina or doped alumina ceramics are commonly used in accelerator environments, not only for beam diagnostics [53] but also for various other functions [54,55]. Changes in the electronic and mechanical properties of alumina ceramics in radiation environments were investigated under both particle and X-ray irradiation in several studies [56–59]. Studies

indicate that electron irradiation induces a reversible yellow discoloration in alumina ceramics by modifying their electronic states, while X-ray exposure does not significantly affect dielectric properties, ensuring continued viability in accelerator environments [60,61]. Notably, alumina ceramics has been used successfully for years in AWAKE for other noninvasive beam diagnostic purposes [42] at repetition rates of up to 10 Hz, with no evidence of degradation caused by secondary electrons or dark current.

The radiators were designed to protrude into the metallic beam pipe to reduce the impact parameter, which increases ChDR intensity but also introduces the possibility of generating diffraction radiation. To address this, the protruding faces were coated with a metallic layer to minimize the generation of diffraction radiation. The metallic coating helps reduce the contribution of background light and also mitigates multipactor effects [62].

Figure 1 shows the temporal evolution of the polarization radiation from one of the radiators in four different time frames, simulated using CST Suite [63] with the parameters given in Table I. One should note that the electron bunch length was chosen as 2 ps and the shortest wavelength spatially sampled at a rate of 10 mesh cells per wavelength due to insufficient computational time and resources. The Coulomb field of the bunch is reflected by the metallic coating of the protruding faces, preventing the generation of DR and ensuring that ChDR is generated from the bottom surface. The only contribution, besides ChDR, is diffraction from the sharp edges. Meanwhile, diffraction from sharp edges is not a background effect contributing to the noise signal but rather a fundamental part of the polarization radiation process, contributing to the width of the ChDR angular distribution. Therefore, it is considered an inherent feature of the ChDR mechanism. Thus, the 3D electromagnetic simulation results show that the optimized radiators allow us to detect the ChDR wavefront as desired. One should note that geometric wakefields are generated behind the Coulomb field due to the finite size of the beam pipe, as well as reflections from sharp edges and faces. The interaction of these wakefields with the
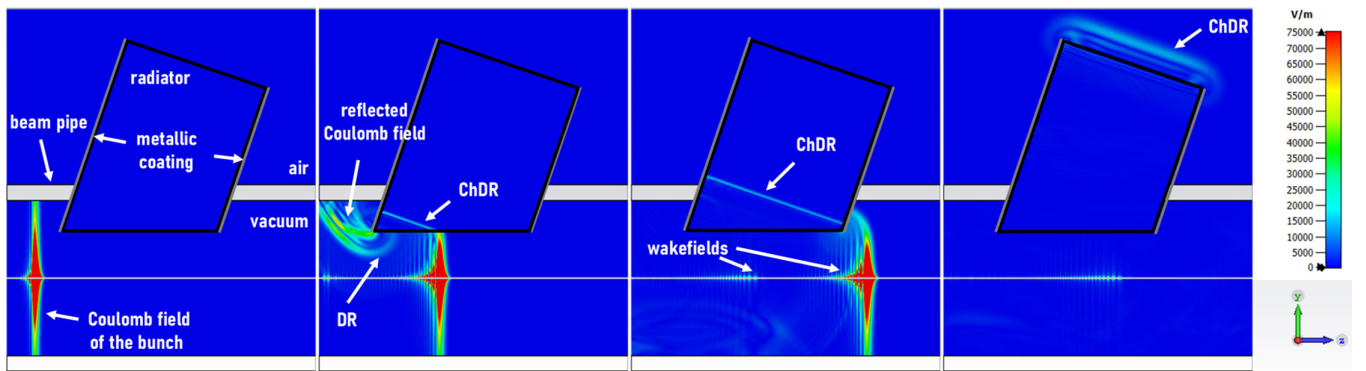

FIG. 1. The temporal evolution of polarization radiation (DR and ChDR) from the 3D model of the optimized radiator is shown at four different time frames along the electron bunch trajectory. The intensity scale in all frames is kept the same to compare the radiation intensities with the Coulomb field. The ChDR wavefront can be observed propagating throughout the radiator. The generation of DR is prevented on the protruding faces thanks to the metallic coating. However, DR production can still be observed in the beam pipe due to the interaction of the Coulomb field with the radiator edges. Geometric wakefields are also observed behind the Coulomb field due to the finite size of the beam pipe and reflections from the sharp edges and the bottom surface of the radiator.

TABLE I. Parameters used for the 3D electromagnetic simulation illustrated in Fig. 1.

Parameter	Value	Unit
Bunch energy	150	MeV
Bunch charge	100	pC
Bunch (temporal) length	2	ps
Radiator dielectric permittivity	9.5	—
Radiator edge length	16.28	mm
Radiator base length	50	mm
Radiator angle	19	°
Impact parameter	15	mm
Beam pipe diameter	50	mm

radiator might result in additional background emission behind the main ChDR wavefront. These contributions are physical but negligibly small to be observed in the experiments. One should also note that the excitations caused by the radiator itself, as it acts as a rectangular waveguide, are naturally filtered because these frequencies are much lower than the detector's response frequency range.

C. Determination of ChDR detectors

The ChDR bunch length measurement technique is a relative measurement based on the ratio of the measured coherent ChDR intensity by two Schottky detectors with different spectral sensitivities. Therefore, the most suitable frequency ranges in which Schottky detectors operate must be optimized. In our approach, one detector generates a normalization parameter, meaning the ChDR intensity changes are negligibly small with changes in bunch length, while the other detector is sensitive to the bunch length. Nevertheless, both detectors are similarly sensitive to the bunch charge. Table II presents a selection of Schottky diode detectors from two vendors, Millitech [64] and Virginia Diodes [65]. The information provided for each detector in the table was used to theoretically calculate the coherent radiation spectrum and intensity, analyze the response of each detector to a range of bunch lengths, and ultimately identify the optimum Schottky pair.

TABLE II. A list of Schottky detectors with their waveguide formats, corresponding frequency ranges, low cut-off frequencies, and associated horn types and dimensions.

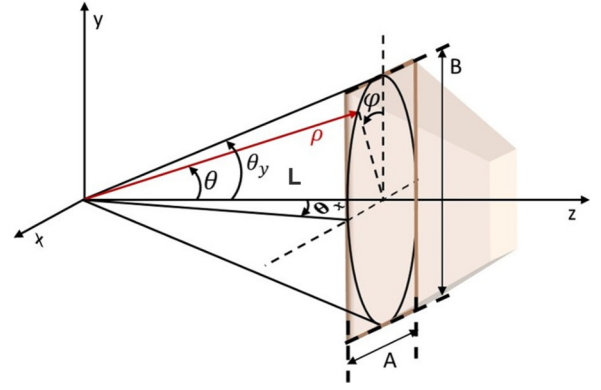| Waveguide (Format)	Frequency (GHz)	Low cut-off (GHz)	Horn (Type)	Dimension (mm × mm)
		Millitech		
WR-15	50–75	39.8	Pyramidal	36.4 × 27.6
WR-12	60–90	48.3	Pyramidal	30.0 × 22.8
WR-10	75–110	59.0	Pyramidal	24.6 × 18.6
WR-08	90–140	73.7	Pyramidal	19.6 × 14.9
		Virginia Diodes		
WR-2.2	325–500	263.0	Diagonal	4.6 × 4.6
WR-1.9	400–600	315.9	Diagonal	3.1 × 3.1
WR-1.5	500–750	394.5	Diagonal	2.4 × 2.4
WR-1.2	600–900	483.5	Diagonal	2.0 × 2.0

FIG. 2. Transformation of the coordinates from spherical to Cartesian considering the horn antenna dimensions of each detector.

To calculate the coherent ChDR spectrum and the radiation captured by the corresponding horn aperture of each Schottky detector, the solid angle, $d\Omega$, needs to be defined by considering the horn dimensions. Therefore, the position of the horn antenna was considered parallel to and centered with respect to the radiator surface for the calculations, as shown in Fig. 2. The horizontal and vertical dimensions of the horn, A and B (as the limit of x and y), can be used to define θ_x and θ_y, respectively. Hence, the coherent ChDR spectrum of a Gaussian electron bunch of N particles can be calculated by integrating the ChDR spectral-angular distribution of a single electron as given below,

$$\frac{dW}{d\omega} = N^2 \exp\left(-\omega^2 \sigma_z^2\right) \int_{\frac{-\theta_x}{2}}^{\frac{\theta_x}{2}} \int_{\theta_{\mathrm{ChDR}}-\frac{\theta_y}{2}}^{\theta_{\mathrm{ChDR}}+\frac{\theta_y}{2}} \frac{d^2W}{d\omega d\Omega} \, d\theta_x \, d\theta_y.$$

(9)

Figure 3 shows the coherent ChDR spectrum and radiation intensity calculated within the operational ranges of Schottky detectors using the bunch and radiator parameters given in Table I for four different bunch lengths: 100, 200, 400, and 600 fs. The total coherent radiation intensity was found by integrating the spectrum over the corresponding frequency range of each detector given in Table II. The diffraction effects dominate the radiation spectrum at lower frequencies, where the coherent radiation intensity is relatively uniform for different bunch lengths. In contrast, at higher frequencies, these effects are suppressed by the bunch form factor, and the bunch length strongly influences the coherent radiation intensity. Thus, the dominance of diffraction effects and the bunch form factor on different parts of the coherent radiation spectrum allows us to select Schottky detectors with the desired functionality. A WR-12 diode from Millitech was selected as the normalization detector, offering a similar response for the entire bunch length range. Regarding the sensitivity detector, two aspects were considered: The detector frequency range should be selected in the frequency region where the coherent ChDR radiation spectrum has the maximum dependence on the bunch length, and the detection range should be wide enough to study the minimum achievable bunch length measurement range.
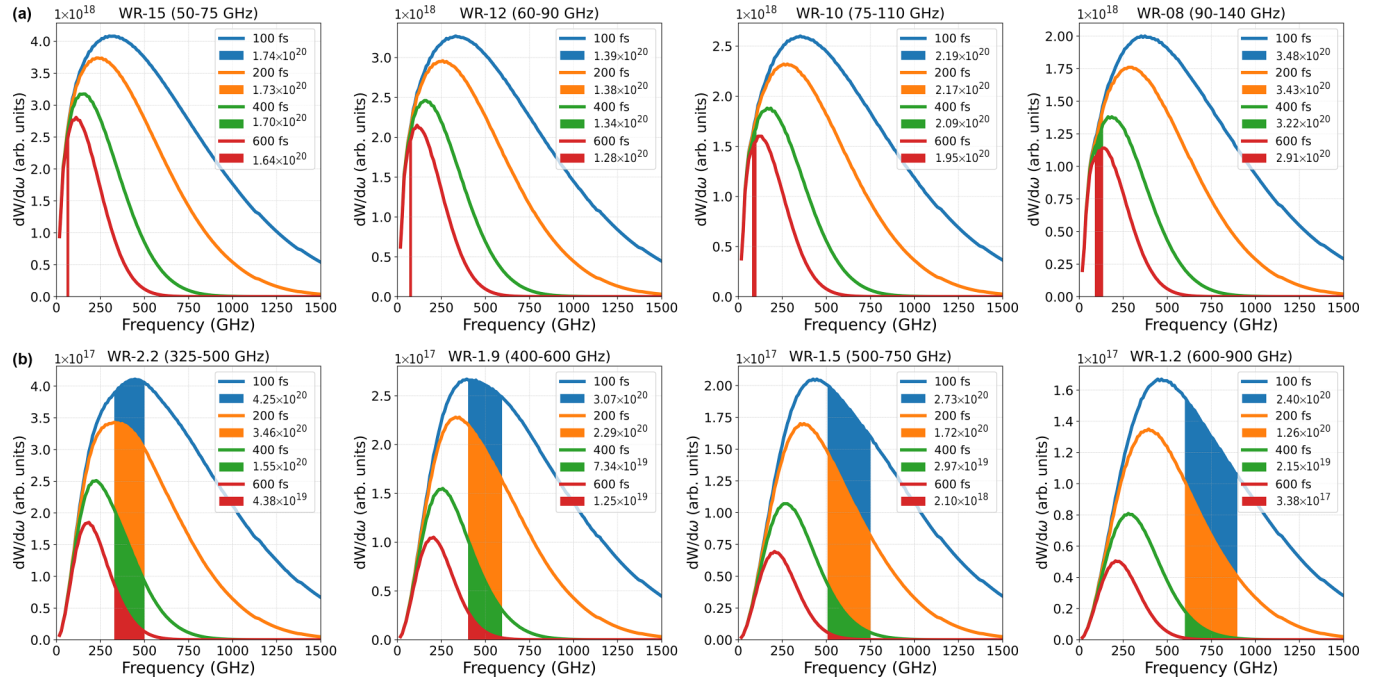
FIG. 3. The coherent ChDR spectrum is calculated for each Schottky detector using (a) Millitech and (b) Virginia diodes, considering the corresponding horn dimensions and operational frequency ranges given in Table II. The waveguide format and frequency range of the corresponding detectors are provided at the top of each plot. The coherent radiation intensity is represented by the area under each spectrum, calculated by integrating the spectrum over the corresponding frequency ranges for different bunch lengths from 100 to 600 fs.

Figure 4 shows the coherent ChDR intensity and the ChDR ratio of the selected detectors for bunch lengths from 100 to 600 fs. The theoretically calculated coherent ChDR intensity for WR-12 is relatively uniform within that range, while WR-1.9 is highly sensitive and shows a large variation in radiation intensity as shown in Fig. 4(a). The ChDR intensity ratio, which directly affects the bunch length calculation, varies between 0.81 and 0.036 within the range as given in Fig. 4(b). Therefore, the WR-12 and WR-1.9 diode detectors were chosen to conduct the experimental campaign, which allows for large dynamic range measurement, providing a highly sensitive bunch length diagnostic tool.

IV. EXPERIMENT AT CLEAR FACILITY

In this section, we describe the standard operation of the electron linac at CLEAR operating at a repetition rate of up to 10 Hz to prepare the short electron bunches and the ChDR data acquisition procedure. We then analyze the experimental data theoretically to discuss the possible impact of the bunch profile on the bunch length calculation.

A. Data acquisition procedure and experimental bunch parameters

The electron bunch is driven from the cathode to the first accelerating structure to compress the bunch via velocity bunching. The cavity phase is adjusted to compress the bunch based on phase and energy correlation. The bunch length is then measured downstream using the radio frequency deflecting (RFD) cavity [66]. The RF field causes a time-varying deflecting force, correlating the bunch deflection with the transverse bunch size and length. A screen measures the transverse size without deflecting voltage, then with $\pm 10°$ deflection in $5°$ steps. The bunch length is then calculated by considering beta functions, bunch energy, deflecting voltage, and phase. Next, the bunch energy is measured, and the alignment is checked using two beam position monitors upstream and downstream of the ChDR setup. Correctors and focusing magnets ensure charge transport upstream of the beam pipe, and the bunch charge is measured and logged shot by shot at the end of the beamline. Once the bunch parameters are checked and logged, ChDR signals are captured by the Schottky detectors located 2 mm away from the radiator surface to
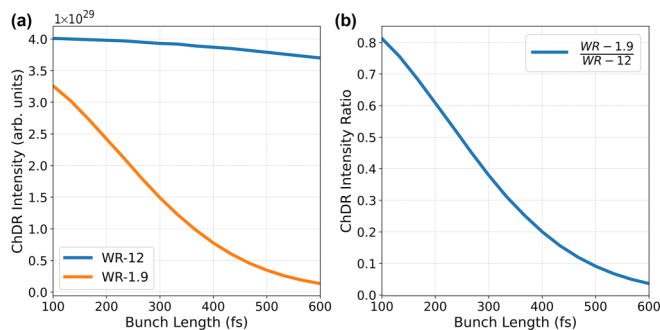

FIG. 4. The theoretical bunch length dependence of (a) coherent ChDR intensity calculated for WR-12 and WR-1.9, and (b) coherent ChDR intensity ratio of the detectors from 100 to 600 fs.

TABLE III. The experimental bunch parameters used to acquire coherent ChDR data set.

Bunch length (ps)	Charge (pC)	Energy (MeV)
0.098 ± 0.002	87.5	167.6
0.162 ± 0.001	88.1	167.9
0.202 ± 0.002	88.6	167.6
0.330 ± 0.009	92.1	167.4
0.411 ± 0.017	95.3	167.4
0.509 ± 0.012	95.1	167.4
0.606 ± 0.022	95.6	167.9
0.704 ± 0.019	100.6	167.5
0.847 ± 0.023	105.9	167.0
0.944 ± 0.069	112.1	167.6
1.021 ± 0.059	110.8	167.3
1.167 ± 0.115	115.5	167.2

prevent cross-talk and capture maximum radiation intensity. The ChDR signals are then transported via coaxial cables to a 10-GHz oscilloscope placed outside the accelerator, registered to the CERN technical network, allowing remote control.

The electron bunch preparation and parameter logging procedure is repeated before each ChDR data acquisition without stopping the accelerator. Table III shows the bunch parameters for each different bunch length measured using the RF deflector to calibrate the ChDR bunch length monitor.

As the WR-12 horn aperture almost covers the radiator exit surface, a 10-dB fixed attenuator was used to avoid the detector saturation. Meanwhile, no waveguide or attenuator was used for the WR-1.9 detector, as its horn aperture is significantly smaller than the radiator exit surface and the horn length is long enough compared to the waveguide aperture to avoid ChDR generated outside the frequency range of the detector. Figure 5 shows the alumina radiators inserted into the beam pipe using flanges. The Schottky detectors were centered on each radiator and were mounted onto an optical breadboard on the CLEAR beamline. One should note that
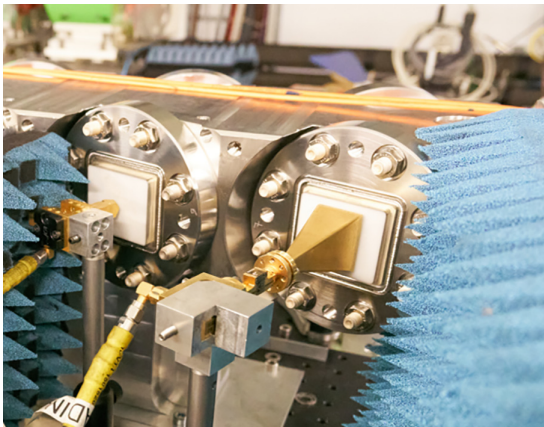

FIG. 5. The two alumina radiators inserted into the beam pipe, the detectors (WR-12 on the right and WR-1.9 on the left) and corresponding horn antennas placed 2 mm away from the radiator face on the CLEAR beamline. The electron bunch travels from right to left.
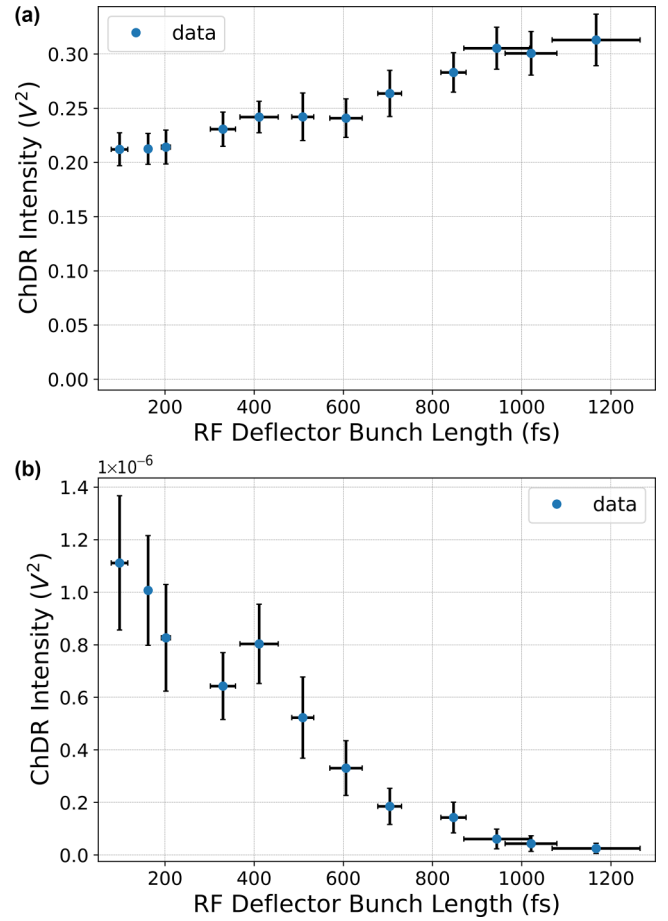

FIG. 6. Coherent ChDR intensity measured by (a) WR-12 and (b) WR-1.9 for each bunch parameter plotted against the bunch length measured by RF deflector. The standard deviation of detected coherent ChDR intensity and RFD bunch length measurements were demonstrated by horizontal and vertical bars.

the shielding between the radiators was removed to better visualize the setup.

Both Schottky detectors operate in the "linear" regime, meaning that the voltage measured by each detector is linearly proportional to the bunch charge. Therefore, the ChDR intensity is proportional to the square of the total bunch charge due to coherency. Consequently, the signal amplitude was measured for each bunch length, and the square of the amplitude was determined as the ChDR intensity. Figure 6 shows the coherent ChDR intensity measured by each detector for each bunch parameter given in Table III. The data points for RFD bunch length and coherent ChDR intensity were obtained using 25 and 300 samples per measurement, respectively. The standard deviation of these measurements was primarily influenced by several factors, including the stability of the klystron, background fluctuations, the number of measurement samples, and the bunch charge, position, and angular jitter for each sample.

Figure 6(a) shows an increase in the coherent radiation intensity detected by WR-12 with the bunch length due to the increasing bunch charge. In Fig. 6(b), the intensity detected by WR-1.9 decays with the increasing bunch length, similar to Fig. 4(a), as the coherent radiation spectrum cannot cover the

entire frequency range of the detector similar to the theoretical calculations shown in Fig. 3 due to the increasing bunch length. However, there is a noticeable increase in the ChDR intensity of the fifth data point compared to the fourth, despite no significant change in charge between these data points. Hence, the possible reason for this increase is a significant change in the longitudinal bunch profile. This change could be due to RF phase and/or field variations while elongating the bunch during the data acquisition campaign, resulting in a shift of the coherent radiation spectrum to higher frequencies and thus increasing the measured coherent radiation intensity.

B. Theoretical analysis of the experimental data

The theoretical investigation of the influence of the longitudinal bunch profile on the experimental data was performed due to our estimations along with previous experiments conducted at the CLEAR facility at CERN [67], which reported the observation of both Gaussian and skew-Gaussian bunch profiles [45,49]. The form factor of a skew-Gaussian bunch is derived in Appendix A and given by

$$F(\omega) = \exp\left(-\omega^2 \sigma_z^2\right) \left| 1 - \text{erf}\left(i \frac{\alpha \sigma_z \omega}{\sqrt{1 + 2\alpha^2}}\right) \right|^2, \quad (10)$$

where α is a dimensionless constant that determines the skewness of the distribution and erf defines the Gauss error function. The sign of α defines the position of skewness either along the rising or falling edge of the distribution. This expression converges to the form factor of Gaussian distribution as given in Eq. (5) when $\alpha = 0$.

Figure 7 shows the experimentally measured and theoretically calculated coherent ChDR intensities. Theoretical results were obtained by calculating the spectrum using the form factor given in Eq. (10) with different skewness parameters for the bunch parameters listed in Table III and integrating the spectrum over the corresponding frequency ranges for each detector. Both experimental and theoretical results were normalized for comparison.

The theoretically calculated coherent ChDR intensity for WR-12, assuming a Gaussian distribution ($\alpha = 0$), does not match the experimental data as shown in Fig. 7(a). However, the model matches the data using a skew-Gaussian profile with $\alpha = 1.5$. The results for WR-1.9 are also consistent with those for WR-12, as shown in Fig. 7(b). The theoretically calculated coherent radiation intensities decay faster than the experimental data for the Gaussian longitudinal profile. The impact of the change in skewness for each measurement is more evident considering the data points below and above the theoretical line calculated for the skew-Gaussian profile with $\alpha = 1.5$.

The theoretical ChDR ratios for Gaussian and skew-Gaussian profiles are given with the experimental ChDR ratios in Fig. 8. The comparison between theoretical results and experimental data indicates that the skewness parameter of each electron bunch listed in Table III used in the ChDR data acquisition campaign varies. Although the longitudinal profile was observed using the RF deflector during the reference bunch length measurements, the raw data could not be delivered for further skewness analysis and comparison.
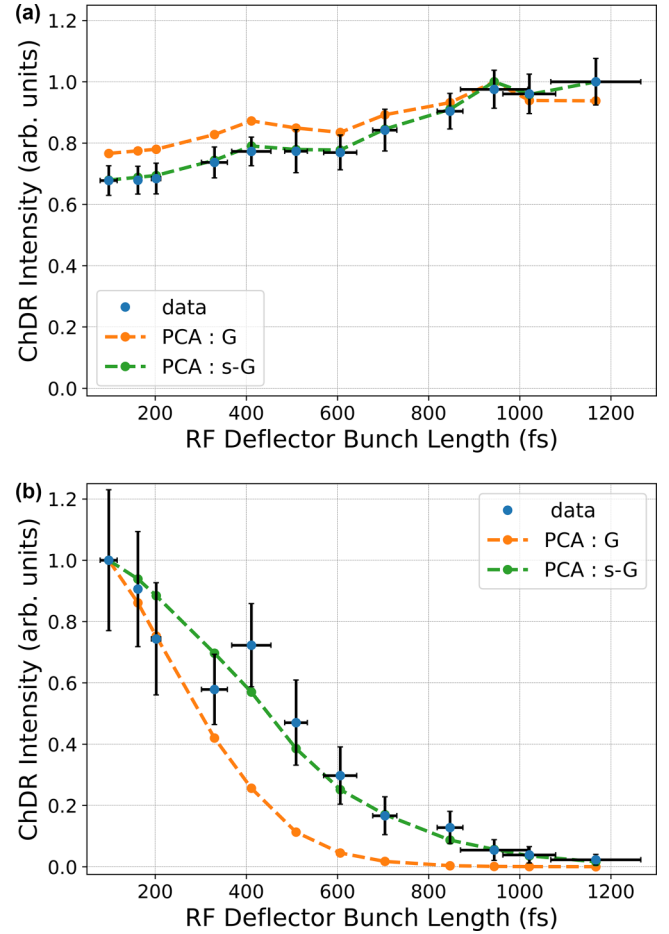

FIG. 7. The experimental data and theoretically calculated ChDR intensity using the bunch parameters given in Table III for different bunch lengths and profiles. Both datasets are normalized to enable a direct comparison. Coherent ChDR intensity is shown (a) for WR-12 (b) for WR-1.9. The dots and lines in blue, orange, and green correspond to experimental data, Gaussian (G), and skew-Gaussian (s-G) distribution with $\alpha = 1.5$, respectively.
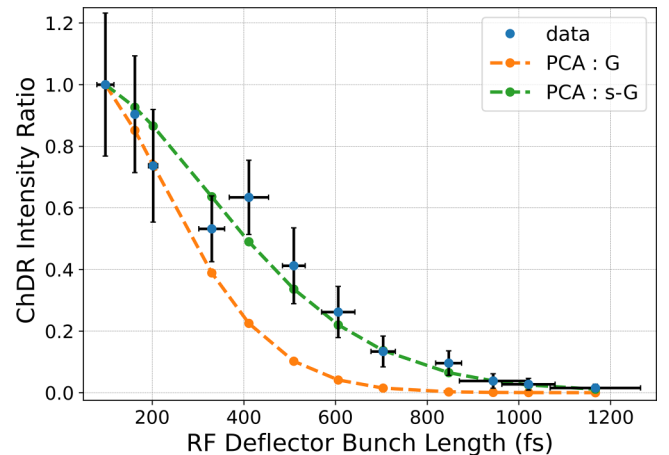

FIG. 8. Normalized coherent ChDR intensity ratio obtained using the experimental and theoretical results shown in Fig. 7.

V. ChDR BUNCH LENGTH MEASUREMENT

Schottky detectors were used without band-pass filters to receive sufficient coherent radiation to measure the bunch length. However, the bunch length calculation technique exploits coherent ChDR radiation measured at a specific frequency, as in Eq. (8). Therefore, the responsivity data provided for each Schottky detector was used to find a weighted average frequency assumed as the ChDR detection frequency for the bunch length calculation. The average responsivity of the detectors was found to be similar. The weighted average responsivity of WR-12 was slightly higher than 2000 V/W, while it was slightly lower than 2000 V/W for WR-1.9. Considering the responsivity data, the weighted average frequency was determined as 76.2 GHz for WR-12 and 503.5 GHz for WR-1.9. Using these frequencies, the coherent ChDR generated by a single electron was calculated, and finally, the ChDR bunch length was determined as shown in Fig. 9.

Although the ChDR bunch length range matches the RFD bunch length range, the measured ChDR bunch length values show an offset. The source of this offset can be attributed to several factors, with one of the main factors being the bunch profile observed in the experiments. Since the determination of ChDR bunch length given in Eq. (8) is derived using the Gaussian form factor, the presence of the error function due to the skew-Gaussian bunch profile must be taken into account. However, the error function prevents extracting the σ_z. Additionally, the influence of the coherent radiation received beyond the frequency ranges of the detectors, as well as the responsivity of the detectors at these bandwidths, any systematic error due to the attenuator used, and additional electronics error can contribute to the offset.

Nevertheless, the ChDR bunch length values are separated into two sets based on the similar linearity of the obtained bunch lengths. Therefore, linear regression was applied to those two data sets to correct the data with the best-fit lines and consider all errors in the detection and misidentification of the bunch length measurement. The best fit for the first data set was $y = 0.8x + 7272.5$, and the goodness of the fit
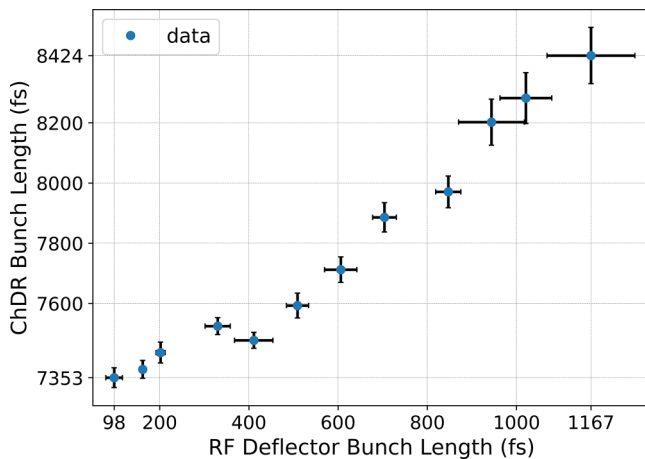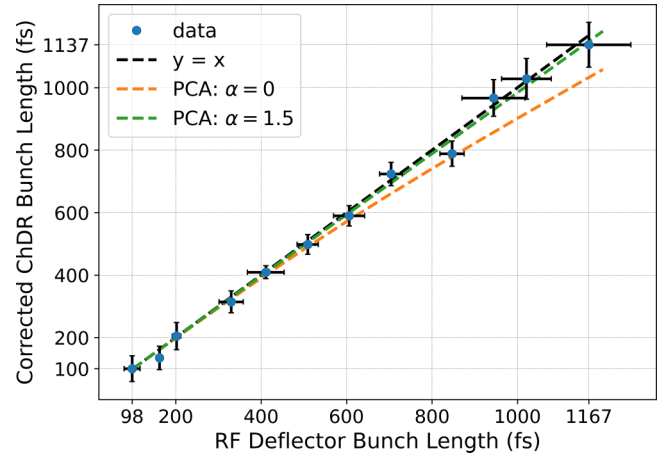

FIG. 10. The ChDR bunch length results against RF deflector bunch lengths after the correction factor applied with the two different lines of the best fit found considering the linear regression applied.

R^2 was 0.98. All data points are within the 95% confidence and prediction interval. The second data set with the best-fit line was $y = 1.3x + 6945.3$, and the R^2 was 0.99.

Figure 10 shows the corrected ChDR bunch lengths with best-fit lines applied to the two data sets, the numerical bunch length results, and the measured RF deflector bunch lengths.

The numerical bunch lengths were calculated using the RFD bunch lengths listed in Table III. These were used to calculate the corresponding form factors at the weighted average frequency of the detectors and eventually determine the ChDR bunch length by dividing each calculated coherent radiation intensity for the detectors. The results confirm the previous findings of having different skewness parameters and validate the applied corrections.

The corrected ChDR bunch lengths were found to be in good agreement with the bunch lengths measured using the RF deflector. Except for one data point, the RF deflector bunch lengths fall within the standard deviation range of the corrected ChDR bunch lengths. Furthermore, the numerical bunch length results indicate that the impact of skewness for short bunch lengths up to 300 fs is negligible. However, the skewness is expected to affect the results for longer bunch lengths, as the numerical results do not match for different longitudinal profiles. Nevertheless, the bunch length monitor is designed for ultrashort bunch lengths and specifically for AWAKE Run 2c, in which the electron bunch length is 200 fs. The closest bunch length used during the tests was 202 ± 10.15 fs with a ± 2.03 fs standard error measured using the RF deflector, which was found to be 204.6 ± 43.53 fs with a ± 2.51 fs standard error using the ChDR bunch length monitor.

VI. DISCUSSION

The current setup is not designed to measure the profile or its skewness, although it has shown sensitivity to the skewness of the longitudinal profile and the bunch length. The observed discrepancies in the data suggest that the sensitivity of the bunch length measurement setup to changes in the bunch

FIG. 9. The measured ChDR bunch length result determined using Eq. (8) are shown against the bunch length measurements using the RF deflector.

profile, along with the actual bandwidth and responsivity of the detectors, can affect the accuracy of the measurements. These limitations could be addressed by enhancing the setup with additional radiators and detectors to improve the capability to measure and analyze the bunch profile and its skewness more accurately if needed.

Although our current analysis focuses on Gaussian and skew-Gaussian bunch profiles—consistent with the design of the diagnostic tool for the AWAKE electron injector and tested at the CLEAR facility—we acknowledge that electron bunches in other accelerators or future experiments may deviate significantly from these shapes. Fortunately, the beam pipe is designed to potentially accommodate up to six radiators simultaneously, offering greater flexibility and higher degrees of freedom for more detailed analysis. By using additional radiators, we can improve single-shot ChDR bunch length measurements by capturing the coherent spectrum across a wider range of frequencies, which would better address non-Gaussian bunch profiles. Alternatively, an interferometric measurement could be performed simultaneously to retrieve the charge distribution and, consequently, the detailed bunch profiles.

Beyond the ChDR bunch length measurement methodology, the use of alumina ceramics has been validated through extensive testing at CLEAR, showing no measurable degradation in diagnostic performance, consistent with other studies using ChDR for beam diagnostic purposes [68–70], where no contrary evidence was observed. Although there is no direct interaction between the electron bunch and the alumina ceramics—since the ChDR bunch length monitor is a noninvasive diagnostic tool—dielectric charging due to dark current or secondary electrons might be a concern in certain accelerator environments where electron clouds are prevalent, such as in high-energy synchrotrons or high repetition-rate accelerators, where additional considerations may be necessary. However, further discussion on the possible limitations of using alumina ceramics due to dielectric charging in such accelerators extends beyond the scope of this paper and requires dedicated research.

VII. CONCLUSION

We demonstrated the design, implementation, and experimental validation of an innovative, noninvasive electron bunch length monitor based on the detection of coherent ChDR emission. The ChDR bunch length measurement technique was tested with a set of bunch lengths ranging from 98 to 1167 fs, as measured by the RF deflector, which served as the invasive gold standard in our experiment. The sensitivity of the measurement technique to both bunch length and profile was demonstrated and validated. The shortest bunch length measured with the RF deflector was 98 ± 18.67 fs with a ± 3.73 fs standard error, while it was found 100.23 ± 41.31 fs with a ± 2.38 fs standard error using the ChDR bunch length monitor. The resolution of the ChDR bunch length setup couldn't be determined or tested due to the limitations of the accelerator and RF deflector resolution. Nevertheless, given the coherent radiation spectrum and intensity, the designed diagnostic tool is estimated to detect bunch lengths in the range of a few tens of femtoseconds.

APPENDIX: DERIVATION OF THE SKEW-GAUSSIAN FORM FACTOR

This Appendix provides the derivation of the bunch form factor of a skew-Gaussian electron bunch to correct the ones provided in the previous publications, ensuring that the error function and the final expression are dimensionless.

The skew-Gaussian distribution is defined as:

$$\text{SkG}(z) = \frac{1}{\sqrt{2\pi}\sigma_z} e^{-\frac{z^2}{2\sigma_z^2}} \left[1 + \text{erf}\left(\frac{\alpha z}{\sigma_z}\right) \right], \quad \text{(A1)}$$

where the dimensionless parameter α gives a measure of the skewness of the distribution. The electron current density $j(z)$ for a skew-Gaussian bunch is then written as:

$$j(z) = j_0 \frac{1}{\sqrt{2\pi}\sigma_z} e^{-\frac{z^2}{2\sigma_z^2}} \left[1 + \text{erf}\left(\frac{\alpha z}{\sigma_z}\right) \right], \quad \text{(A2)}$$

where j_0 is the peak current density. The coherent radiation spectrum, $\frac{dI}{d\omega}$, is emitted by this electron bunch and is proportional to $|j(\omega, \sigma_z, \alpha)|^2$, where $j(\omega, \sigma_z, \alpha)$ is the Fourier transform of the electron current density which is written as below:

$$j(\omega, \sigma_z, \alpha) = j_0 \frac{1}{\sqrt{2\pi}\sigma_z} \int_{-\infty}^{\infty} e^{-\frac{z^2}{2\sigma_z^2}} \left[1 + \text{erf}\left(\frac{\alpha z}{\sigma_z}\right) \right] e^{-i\omega z} dz. \quad \text{(A3)}$$

Thus, the integral can be separated into two parts:

$$j(\omega, \sigma_z, \alpha) = j_0 \frac{1}{\sqrt{2\pi}\sigma_z} \Bigg(\int_{-\infty}^{\infty} e^{-\frac{z^2}{2\sigma_z^2}} e^{-i\omega z} dz$$
$$+ \int_{-\infty}^{\infty} e^{-\frac{z^2}{2\sigma_z^2}} \text{erf}\left(\frac{\alpha z}{\sigma_z}\right) e^{-i\omega z} dz \Bigg), \quad \text{(A4)}$$

where the first part of Eq. (A4) gives

$$\int_{-\infty}^{\infty} e^{-\frac{z^2}{2\sigma_z^2}} e^{-i\omega z} dz = \sqrt{2\pi}\sigma_z e^{-\frac{\sigma_z^2 \omega^2}{2}}, \quad \text{(A5)}$$

as a result of the Gaussian integral. The second part of Eq. (A4) involving the error function can be written as the

combination of the terms in the arguments of the exponential functions to obtain the following expression:

$$\int_{-\infty}^{\infty} e^{-\frac{z^2}{2\sigma_z^2}} \, \text{erf}\left(\frac{\alpha z}{\sigma_z}\right) e^{-i\omega z} dz$$

$$= e^{-\frac{\sigma_z^2 \omega^2}{2}} \int_{-\infty}^{\infty} e^{-\frac{1}{2}\left(\frac{z}{\sigma_z} + i\sigma_z\omega\right)^2} \text{erf}\left(\frac{\alpha z}{\sigma_z}\right) dz. \qquad (A6)$$

Now we derive the integral expression in Eq. (A6) by first differentiating with respect to ω leaving the $e^{-\frac{\sigma_z^2\omega^2}{2}}$ term out:

$$\frac{\partial}{\partial\omega}\left(\int_{-\infty}^{\infty} e^{-\frac{1}{2}\left(\frac{z}{\sigma_z}+i\sigma_z\omega\right)^2} \text{erf}\left(\frac{\alpha z}{\sigma_z}\right) dz\right)$$

$$= -i\sigma_z \int_{-\infty}^{\infty} e^{-\frac{1}{2}\left(\frac{z}{\sigma_z}+i\sigma_z\omega\right)^2} \left(\frac{z}{\sigma_z} + i\sigma_z\omega\right) \text{erf}\left(\frac{\alpha z}{\sigma_z}\right) dz. \qquad (A7)$$

The expression above can then be integrated by parts:

$$i\sigma_z^2 e^{-\frac{1}{2}\left(\frac{z}{\sigma_z}+i\sigma_z\omega\right)^2} \text{erf}\left(\frac{\alpha z}{\sigma_z}\right)\Bigg|_{-\infty}^{\infty}$$

$$- \frac{2i\alpha\sigma_z}{\sqrt{\pi}} \int_{-\infty}^{\infty} e^{-\frac{1}{2}\left(\frac{z}{\sigma_z}+i\sigma_z\omega\right)^2} e^{-\frac{\alpha^2 z^2}{\sigma_z^2}} dz. \qquad (A8)$$

The first term of integration by parts vanishes while the second term can be integrated with respect to z to get:

$$-\frac{2i\alpha\sigma_z}{\sqrt{\pi}} \int_{-\infty}^{\infty} e^{-\frac{1}{2}\left(\frac{z}{\sigma_z}+i\sigma_z\omega\right)^2} e^{-\frac{\alpha^2 z^2}{\sigma_z^2}} dz = -\frac{2\sqrt{2}i\alpha\sigma_z^2}{\sqrt{1+2\alpha^2}} e^{\frac{\alpha^2\sigma_z^2\omega^2}{1+2\alpha^2}}. \qquad (A9)$$

Now we integrate with respect to ω and obtain the expression:

$$-\frac{2\sqrt{2}i\alpha\sigma_z^2}{\sqrt{1+2\alpha^2}} \int_0^\omega e^{\frac{\alpha^2\sigma_z^2\omega^2}{1+2\alpha^2}} d\omega = -\sqrt{2\pi}\,\sigma_z \, \text{erf}\left(\frac{i\alpha\sigma_z\omega}{1+\sqrt{2\alpha^2}}\right). \qquad (A10)$$

Finally multiplying Eq. (A10) with the exponential term we left out in Eq. (A6), we get the final expression for the second part of Eq. (A4):

$$-\sqrt{2\pi}\sigma_z e^{-\frac{\sigma_z^2\omega^2}{2}} \, \text{erf}\left(\frac{i\alpha\sigma_z\omega}{1+\sqrt{2\alpha^2}}\right). \qquad (A11)$$

Combining Eq. (A5) with Eq. (A11) we reach the expression for $j(\omega, \sigma_z, \alpha)$:

$$j(\omega, \sigma_z, \alpha) = j_0 \frac{1}{\sqrt{2\pi}\sigma_z}\left(\sqrt{2\pi}\sigma_z e^{-\frac{\sigma_z^2\omega^2}{2}}\right.$$

$$\left. - \sqrt{2\pi}\sigma_z e^{-\frac{\sigma_z^2\omega^2}{2}} \, \text{erf}\left(\frac{i\alpha\sigma_z\omega}{1+\sqrt{2\alpha^2}}\right)\right). \qquad (A12)$$

After simplification, we obtain the final expression for the skew-Gaussian electron current density as:

$$j(\omega, \sigma_z, \alpha) = j_0 e^{-\frac{\sigma_z^2\omega^2}{2}}\left(1 - \text{erf}\left(\frac{i\alpha\sigma_z\omega}{1+\sqrt{2\alpha^2}}\right)\right). \qquad (A13)$$

The bunch form factor, $F(\omega)$, is finally defined as the absolute square of Eq. (A13), and written as:

$$F(\omega) = e^{-\sigma_z^2\omega^2}\left|1 - \text{erf}\left(i\frac{\alpha\sigma_z\omega}{\sqrt{1+2\alpha^2}}\right)\right|^2. \qquad (A14)$$

[1] R. Assmann *et al.*, Proton-driven plasma wakefield acceleration: A path to the future of high-energy particle physics, Plasma Phys. Control. Fusion **56**, 084013 (2014).

[2] E. Gschwendtner *et al.*, AWAKE, the advanced proton driven plasma wakefield acceleration experiment at CERN, Nucl. Instrum. Methods A **829**, 76 (2016).

[3] A. Caldwell *et al.*, Path to AWAKE: Evolution of the concept, Nucl. Instrum. Methods A **829**, 3 (2016).

[4] P. Muggli *et al.* (AWAKE Collaboration), AWAKE readiness for the study of the seeded self-modulation of a 400 GeV proton bunch, Plasma Phys. Control. Fusion **60**, 014046 (2018).

[5] P. Chen, J. M. Dawson, R. W. Huff, and T. Katsouleas, Acceleration of electrons by the interaction of a bunched electron beam with a plasma, Phys. Rev. Lett. **54**, 693 (1985).

[6] J. B. Rosenzweig, D. B. Cline, B. Cole, H. Figueroa, W. Gai, R. Konecny, J. Norem, P. Schoessow, and J. Simpson, Experimental observation of plasma wake-field acceleration, Phys. Rev. Lett. **61**, 98 (1988).

[7] A. Caldwell, J. Chappell, P. Crivelli, E. Depero, J. Gall, S. Gninenko, E. Gschwendtner, A. Hartin, F. Keeble, J. Osborne, A. Pardons, A. Petrenko, A. Scaachi, and M. Wing, Particle physics applications of the AWAKE acceleration scheme, arXiv:1812.11164.

[8] M. Wing, Particle physics experiments based on the AWAKE acceleration scheme, Philos. Trans. R. Soc. A **377**, 20180185 (2019).

[9] E. Gschwendtner *et al.*, *AWAKE++: The AWAKE Acceleration Scheme for New Particle Physics Experiments at CERN*, Technical Report (CERN, Geneva, 2018).

[10] P. Muggli and for the AWAKE collaboration, Physics to plan AWAKE run 2, J. Phys.: Conf. Ser. **1596**, 012008 (2020).

[11] L. Verra, G. Z. D. Porta, J. Pucek, T. Nechaeva, S. Wyler, M. Bergamaschi, E. Senes, E. Guran, J. T. Moody, M. A. Kedves, E. Gschwendtner, P. Muggli *et al.* (AWAKE Collaboration), Controlled growth of the self-modulation of a relativistic proton bunch in plasma, Phys. Rev. Lett. **129**, 024802 (2022).

[12] E. Gschwendtner, K. Lotov, P. Muggli, M. Wing *et al.* (AWAKE Collaboration), The AWAKE run 2 programme and beyond, Symmetry **14**, 1680 (2022).

[13] R. Akre, L. Bentson, P. Emma, and P. Krejcik, Bunch length measurements using a transverse RF deflecting structure in the SLAC linac, in *Proceedings of the 8th European Particle Accelerator Conference (EPAC 2002)* (Paris, France, 2002), pp. 1882–1884.

[14] R. Pan, A. Andersson, W. Farabolini, A. Goldblatt, T. Lefevre, M. Martyanov, S. Mazzoni, L. Timeo, S. Rey, S. Jamison, W.

Gillespie, and D. Walsh, Electro-optical bunch profile measurement at CTF3, in *4th International Particle Accelerator Conference (IPAC 2013)* (Shanghai, China, 2013), pp. 658–660.

[15] P. Karataev, K. Fedorov, G. Naumenko, K. Popov, A. Potylitsyn, and A. Vukolov, Ultra-monochromatic far-infrared cherenkov diffraction radiation in a super-radiant regime, Sci. Rep. **10**, 20961 (2020).

[16] Y. Glinec, J. Faure, A. Norlin, A. Pukhov, and V. Malka, Observation of fine structures in laser-driven electron beams using coherent transition radiation, Phys. Rev. Lett. **98**, 194801 (2007).

[17] I. Nozawa, K. Kan, J. Yang, A. Ogata, T. Kondoh, M. Gohdo, K. Norizawa, H. Kobayashi, H. Shibata, S. Gonda, and Y. Yoshida, Measurement of $< 20\,\mathrm{fs}$ bunch length using coherent transition radiation, Phys. Rev. ST Accel. Beams **17**, 072803 (2014).

[18] V. Ginzburg, Transition radiation and transition scattering, Phys. Scr. **1982**, 182 (1982).

[19] M. L. Ter-Mikaelian, *High-energy electromagnetic processes in condensed media*, Interscience Tracts on Physics and Astronomy (John Wiley & Sons, New York, 1972).

[20] S. Wesch, B. Schmidt, C. Behrens, H. Delsim-Hashemi, and P. Schmüser, A multi-channel THz and infrared spectrometer for femtosecond electron bunch diagnostics by single-shot spectroscopy of coherent radiation, Nucl. Instrum. Methods A **665**, 40 (2011).

[21] T. J. Maxwell, C. Behrens, Y. Ding, A. S. Fisher, J. Frisch, Z. Huang, and H. Loos, Coherent-radiation spectroscopy of few-femtosecond electron bunches using a middle-infrared prism spectrometer, Phys. Rev. Lett. **111**, 184801 (2013).

[22] T. Kövener, THz spectrometer calibration at FELIX, Ph.D. thesis, Universität Hamburg, Fachbereich Physik, 2016.

[23] T. Muto, S. Araki, R. Hamatsu, H. Hayano, T. Hirose, P. Karataev, G. Naumenko, A. Potylitsyn, and J. Urakawa, Observation of incoherent diffraction radiation from a single-edge target in the visible-light region, Phys. Rev. Lett. **90**, 104801 (2003).

[24] D. Xiang and W.-H. Huang, Ultrashort electron bunch length measurement with diffraction radiation deflector, Phys. Rev. ST Accel. Beams **10**, 012801 (2007).

[25] L. Sukhikh, G. Kube, A. Potylitsyn, and V. Schlott, Coherent resonant diffraction radiation from inclined grating as a tool for bunch length diagnostics, in *Proceedings of the 10th European Workshop on Beam Diagnostics and Instrumentation for Particle Accelerators (DIPAC'11)* (Hamburg, Germany, 2011), pp. 377–379.

[26] G. Doucas, M. F. Kimmitt, A. Doria, G. P. Gallerano, E. Giovenale, G. Messina, H. L. Andrews, and J. H. Brownell, Determination of longitudinal bunch shape by means of coherent smith-purcell radiation, Phys. Rev. ST Accel. Beams **5**, 072802 (2002).

[27] H. L. Andrews, F. B. Taheri, J. Barros, R. Bartolini, V. Bharadwaj, C. Clarke, N. Delerue, G. Doucas, N. Fuster-Martinez, M. Vieille-Grosjean, I. V. Konoplev, M. Labat, S. Le Corre, C. Perry, A. Reichold, and S. Stevenson, Reconstruction of the time profile of 20.35 GeV, subpicosecond long electron bunches by means of coherent smith-purcell radiation, Phys. Rev. ST Accel. Beams **17**, 052802 (2014).

[28] I. V. Konoplev, A. W. Cross, and A. D. R. Phelps, Relativistic electron beam excitation of surface fields in artificial materials based on one- and two-dimensional periodic structures, IEEE Trans. Plasma Sci. **39**, 2610 (2011).

[29] I. V. Konoplev, P. MacInnes, A. W. Cross, A. D. R. Phelps, and K. Ronald, Study of one-dimensional Bragg structures with localized defect, Appl. Phys. Lett. **91**, 171107 (2007).

[30] I. V. Konoplev, L. Fisher, K. Ronald, A. W. Cross, A. D. R. Phelps, C. W. Robertson, and M. Thumm, Surface-field cavity based on a two-dimensional cylindrical lattice, Appl. Phys. Lett. **96**, 231111 (2010).

[31] I. V. Konoplev, G. Doucas, H. Harrison, A. J. Lancaster, and H. Zhang, Single shot, nondestructive monitor for longitudinal subpicosecond bunch profile measurements with femtosecond resolution, Phys. Rev. Accel. Beams **24**, 022801 (2021).

[32] R. Lai and A. Sievers, On using the coherent far IR radiation produced by a charged-particle bunch to determine its shape: I analysis, Nucl. Instrum. Methods A **397**, 221 (1997).

[33] R. W. Gerchberg, A practical algorithm for the determination of phase from image and diffraction plane pictures, Optik **35**, 237 (1972).

[34] A. Curcio, M. Bergamaschi, R. Corsini, D. Gamba, W. Farabolini, T. Lefevre, S. Mazzoni, V. Dolci, M. Petrarca, and S. Lupi, Beam-based sub-THz source at the CERN linac electron accelerator for research facility, Phys. Rev. Accel. Beams **22**, 020402 (2019).

[35] T. Lefevre *et al.*, Non-invasive beam diagnostics with Cherenkov diffraction radiation, in *Proceedings of the 9th International Particle Accelerator Conference (IPAC 2018)*, (Vancouver, BC, Canada, 2018), pp. 2005–2008.

[36] S. Ninomiya *et al.*, Measurement of Cherenkov diffraction radiation from a short electron bunch at t-ACTS, in *Proceedings of the 10th International Particle Accelerator Conference (IPAC 2019)* (Melbourne, Australia, 2019), pp. 2536–2538.

[37] T. Lefèvre *et al.*, Cherenkov diffraction radiation as a tool for beam diagnostics, in *Proceedings of the 8th International Beam Instrumentation Conference (IBIC2019)* (Malmö, Sweden, 2019), pp. 660–664.

[38] M. Bergamaschi *et al.*, Recent results using incoherent Cherenkov Diffraction Radiation for non-invasive beam diagnostics, in *Proceedings of the 10th International Particle Accelerator Conference (IPAC 2019)* (Melbourne, Australia, 2019), pp. 2654–2657.

[39] K. Łasocha *et al.*, Experimental verification of several theoretical models for ChDR description, in *Proceedings of 13th International Particle Accelerator Conference (IPAC 2022)* (Bangkok, Thailand, 2022), pp. 2420–2423.

[40] E. Senes, Development of a beam position monitor for co-propagating electron and proton beams, Ph.D. thesis, Oxford University, 2020.

[41] K. Fedorov, P. Karataev, Y. Saveliev, T. Pacey, A. Oleinik, M. Kuimova, and A. Potylitsyn, Development of longitudinal beam profile monitor based on coherent transition radiation effect for CLARA accelerator, J. Instrum. **15** (06), C06008 (2020).

[42] E. Senes, M. Krupa, S. Mazzoni, K. Lasocha, T. Lefevre, A. Schloegelhofer, M. Wendt, C. Davut, P. Karataev, C. Pakuza, and B. Spear, Selective electron beam sensing through coherent Cherenkov diffraction radiation, Phys. Rev. Res. **6**, 023278 (2024).

[43] M. Amusia, Atomic Bremsstrahlung: Retrospectives, current status and perspectives, Radiat. Phys. Chem. **75**, 1232 (2006).

[44] M. Shevelev and A. S. Konkov, Peculiarities of the generation of Vavilov-Cherenkov radiation induced by a charged particle moving past a dielectric target, J. Exp. Theor. Phys. **118**, 501 (2014).

[45] K. Lasocha, Non-invasive beam diagnostics with Schottky signals and Cherenkov diffraction radiation, Ph.D. thesis, Jagiellonian University, 2022.

[46] J. S. Nodvick and D. S. Saxon, Suppression of coherent radiation by electrons in a synchrotron, Phys. Rev. **96**, 180 (1954).

[47] A. P. Potylitsyn, M. I. Ryazanov, M. N. Strikhanov, and A. A. Tishchenko, Diffraction radiation from relativistic particles, Springer Tracts Mod. Phys. **239**, 1 (2011).

[48] R. Ramjiawan, V. Bencini, P. Burrows, and F. Velotti, Design of the proton and electron transfer lines for AWAKE Run 2c, Nucl. Instrum. Methods A **1049**, 168094 (2023).

[49] A. Curcio, M. Bergamaschi, R. Corsini, W. Farabolini, D. Gamba, L. Garolfi, R. Kieffer, T. Lefevre, S. Mazzoni, K. Fedorov *et al.*, Noninvasive bunch length measurements exploiting Cherenkov diffraction radiation, Phys. Rev. Accel. Beams **23**, 022802 (2020).

[50] Morgan Advance Materials, AL-300.

[51] K. Z. Rajab, M. Naftaly, E. H. Linfield, J. C. Nino, D. J. Arenas, D. B. Tanner, R. Mittra, and M. T. Lanagan, Broadband dielectric characterization of aluminum oxide (AL2O3), J. Microelectron. Electron. Packag. **5**, 2 (2008).

[52] K. Berdel, J. G. Rivas, P. H. Bolívar, P. de Maagt, and H. Kurz, Temperature dependence of the permittivity and loss tangent of high-permittivity materials at terahertz frequencies, IEEE Trans. Microwave Theory Tech. **53**, 1266 (2005).

[53] M. Jana, M. Chung, B. Freemire, P. Hanlet, M. Leonova, A. Moretti, M. Palmer, T. Schwarz, A. Tollestrup, Y. Torun *et al.*, Measurement of transmission efficiency for 400 MeV proton beam through collimator at Fermilab MuCool test area using chromox-6 scintillation screen, Rev. Sci. Instrum. **84**, 063301 (2013).

[54] W. Kalbreier and B. Goddard, Radiation-triggered breakdown phenomena in high-energy e/sup+/e/sup-/colliders, IEEE Trans. Electr. Insul. **28**, 444 (1993).

[55] S. Michizono, Y. Saito, S. Fukuda, K. Hayashi, and S. Anami, RF windows used at S-band pulsed klystrons in the KEK linac, Vacuum **47**, 625 (1996).

[56] N. E. F. Othman, Y. Abdullah, H. Purwanto, and K. H. Zaini, Effect of electron beam irradiation on the morphology of alumina ceramic, Adv. Mater. Res. **1115**, 142 (2015).

[57] K. Nagabhushana, B. Lakshminarasappa, and F. Singh, Photoluminescence and Raman studies in swift heavy ion irradiated polycrystalline aluminum oxide, Bull. Mater. Sci. **32**, 515 (2009).

[58] D. White, L. Snead, S. Zinkle, and W. Eatherly, *In situ* measurement of radiation induced conductivity in oxide insulators during neutron irradiation, J. Appl. Phys. **83**, 1924 (1998).

[59] F. Gastou and M. Fichet, Radiation induced conductivity and relation with space charge in Al_2O_3 (ceramic and sapphire), in *Proceedings of the 1995 Conference on Electrical Insulation and Dielectric Phenomena* (IEEE, Los Alamitos, CA, 1995), pp. 320–322.

[60] M. Kinsho, Y. Saito, D. Nishizawa, and S. Michizono, 2.5 MeV electron irradiation effect of alumina ceramics, J. Nucl. Mater. **318**, 307 (2003).

[61] P. Gan, X. Yi, M. Li, Y. Lei, D. Jin, and L. Chen, Effect of x-ray irradiation on the properties of alumina ceramics, J. Instrum. **15**, T09007 (2020).

[62] S. Michizono, Y. Saito, Y. Yamano, S. Kobayashi *et al.*, Secondary electron emission of tin-coated alumina ceramics, Vacuum **81**, 762 (2007).

[63] Dassault Systems, CST Studio Suite.

[64] Smiths Interconnect, Millitech diodes.

[65] Virginia Diodes, Inc., Virginia diodes.

[66] A. Gilardi, Measurements of wakefields and bunch length with beam in linear electron accelerators: A case study at the CLEAR facility, Ph.D. thesis, Naples University, 2021.

[67] D. Gamba, R. Corsini, S. Curt, S. Doebert, W. Farabolini, G. Mcmonagle, P. Skowronski, F. Tecker, S. Zeeshan, E. Adli, C. Lindstrøm, A. Ross, and L. Wroe, The CLEAR user facility at CERN, Nucl. Instrum. Methods A **909**, 480 (2018).

[68] C. Pakuza *et al.*, Electron beam studies on a beam position monitor based on Cherenkov diffraction radiation, in *Proceedings of 14th International Particle Accelerator Conference (IPAC 2023)* (Venice, Italy, 2023), pp. 4806–4809.

[69] A. Schloegelhofer, Non-invasive beam diagnostic development for FCC using cherenkov diffraction radiation in dielectric materials, Ph.D. thesis, Vienna, Tech. University, 2024.

[70] B. Spear *et al.*, Beam studies using a Cherenkov diffraction based beam position monitor for AWAKE, in *Proceedings of 15th International Particle Accelerator Conference (IPAC 2024)* (Nashville, TN, 2023), pp. 2327–2330.